Migration velocity analysis based on linearization of the two-way wave equation

Ali Almomin and Yaxun Tang

ABSTRACT

Wave equation migration velocity analysis (WEMVA) is a family of techniques that aims to improve the subsurface velocity model by minimizing the residual in image space. This process is performed iteratively by linearizing the imaging operator in order to relate image perturbations to model updates. This linearization is conventionally based on the one-way wave equation, which has some pitfalls in terms of accuracy and ability to image certain wavepaths in complex geology. We present a formulation of WEMVA based on the two-way wave equation which can improve the accuracy of the model estimate. There are two approximations used to linearize this operator. First is the Born approximation and the second envolves dropping the second order slowness perturbation term. In this paper, we show preliminary results of using the two-way based WEMVA, as well as the resolution matrix of the operator.

INTRODUCTION

Seismic velocity analysis methods can be divided into two major groups. First, there are techniques that aim at minimizing the misfit in the data domain such as full waveform inversion (Tarantola, 1984; Luo and Schuster, 1990; Biondi, 2009). Second, there are other techniques that aim at improving the quality in the image domain such as migration velocity analysis (MVA)(Symes and Carazzone, 1991; Biondi and Sava, 1999; Shen, 2004). These techniques try to measure the quality of the image several ways and then invert the estimated image perturbation using a linearized wave equation operator. This tomographic operator is based on a Taylor expansion of the image around a background slowness model.

There are several advantages to minimizing the residual in image-space, such as increasing signal-to-noise ratio and decreasing the complexity of the data (Tang et al., 2008). The linearization in WEMVA is conventionally done based on the one-way wave equation. This approach has some advantages, such as the computational efficiency of one-way wave equation operators. However, it also suffers from disadvantages such as decreased accuracy or the inability to model wide-angle propagations.

In this paper, we show the derivation of a linearized tomographic operator that is based on the two-way wave equation. This operator is the essential part in constructing the gradient of any two-way wave equation based MVA, such as WEMVA by residual moveout fitting (Biondi, 2010). The two-way wave equation is linearized over slowness by dropping the second order slowness perturbation term. Also, the Born approximation is used to derive this operator. We also show a few ways to interpret and implement this operator. Finally, we show the resolution matrix of this operator.

THEORY

First, we start with the imaging condition as the following:

$$I(\mathbf{x},\mathbf{h}) = \sum_{\omega,\mathbf{x}_s,\mathbf{x}_r} G^*(\mathbf{x}-\mathbf{h},\mathbf{x}_s,\omega)G^*(\mathbf{x}+\mathbf{h},\mathbf{x}_r,\omega)d(\mathbf{x}_r,\mathbf{x}_s,\omega), \tag{1}$$

where I is the image, G is the Green's function, d is the surface data, $\mathbf{x}_s$ and $\mathbf{x}_r$ are the source and receiver coordinates, $\mathbf{h}$ is the subsurface offset, $\mathbf{x}$ is the Green's functions' coordinate and ω is frequency. Next, we define the Green's functions based on the two-way wave equation as follows:

$$\left(\nabla^2 + \omega^2 s^2(\mathbf{x})\right) G(\mathbf{x},\mathbf{x}_s,\omega) = -\delta(\mathbf{x}-\mathbf{x}_s), \tag{2}$$

$$\left(\nabla^2 + \omega^2 s^2(\mathbf{x})\right) G(\mathbf{x},\mathbf{x}_r,\omega) = -\delta(\mathbf{x}-\mathbf{x}_r), \tag{3}$$

where s is slowness. Then, we can obtain the derivative of I with respect to the slowness as follows;

$$\begin{aligned}\frac{\partial I(\mathbf{x},\mathbf{h})}{\partial s(\mathbf{y})} = &\sum_{\omega,\mathbf{x}_s,\mathbf{x}_r} \left(\frac{\partial G(\mathbf{x}-\mathbf{h},\mathbf{x}_s,\omega)}{\partial s(\mathbf{y})}\right)^* G^*(\mathbf{x}+\mathbf{h},\mathbf{x}_r,\omega)d(\mathbf{x}_r,\mathbf{x}_s,\omega) \\ &+ \sum_{\omega,\mathbf{x}_s,\mathbf{x}_r} G^*(\mathbf{x}-\mathbf{h},\mathbf{x}_s,\omega)\left(\frac{\partial G(\mathbf{x}+\mathbf{h},\mathbf{x}_r,\omega)}{\partial s(\mathbf{y})}\right)^* d(\mathbf{x}_r,\mathbf{x}_s,\omega),\end{aligned} \tag{4}$$

where $\mathbf{y}$ is the slowness coordinate. Now, we can perturb the slowness:

$$s(\mathbf{x}) = s_0(\mathbf{x}) + \Delta s(\mathbf{x}), \tag{5}$$

where s_0 is the background slowness. Then, we apply a first order approximation by squaring the slowness and ignoring the second order perturbation term as follows:

$$s^2(\mathbf{x}) \approx s_0^2(\mathbf{x}) + 2s_0(\mathbf{x})\Delta s(\mathbf{x}). \tag{6}$$

We define a background Green's function that corresponds to the background slowness:

$$\left(\nabla^2 + \omega^2 s_0^2(\mathbf{x})\right) G_0(\mathbf{x},\mathbf{x}_s,\omega) = -\delta(\mathbf{x}-\mathbf{x}_s). \tag{7}$$

By substituting this into the original wave equation, we arrive at the following:

$$\left(\nabla^2 + \omega^2 s_0^2(\mathbf{x})\right) G(\mathbf{x}, \mathbf{x}_s, \omega) = -2\omega^2 s_0(\mathbf{x}) \Delta s(\mathbf{x}) G(\mathbf{x}, \mathbf{x}_s, \omega) - \delta(\mathbf{x} - \mathbf{x}_s). \tag{8}$$

Now, we apply Born's approximation to simplify the previous equation to the following expression:

$$\left(\nabla^2 + \omega^2 s_0^2(\mathbf{x})\right) \Delta G(\mathbf{x}, \mathbf{x}_s, \omega) = -2\omega^2 s_0(\mathbf{x}) \Delta s(\mathbf{x}) G_0(\mathbf{x}, \mathbf{x}_s, \omega), \tag{9}$$

where ΔG is the perturbed Green's function. Then, we solve for the perturbed Green's function as follows:

$$\Delta G(\mathbf{x}, \mathbf{x}_s, \omega) = -2\omega^2 \sum_{\mathbf{y}} s_0(\mathbf{y}) G_0(\mathbf{y}, \mathbf{x}_s, \omega) \Delta s(\mathbf{y}) G_0(\mathbf{x}, \mathbf{y}, \omega), \tag{10}$$

which enables us to find the derivative of the Green's function with respect to slowness as shown in the following:

$$\frac{\partial G(\mathbf{x}, \mathbf{x}_s, \omega)}{\partial s(\mathbf{y})} = -2\omega^2 s_0(\mathbf{y}) G_0(\mathbf{y}, \mathbf{x}_s, \omega) G_0(\mathbf{x}, \mathbf{y}, \omega). \tag{11}$$

We can follow the same steps for the receiver Green's function to get:

$$\frac{\partial G(\mathbf{x}, \mathbf{x}_r, \omega)}{\partial s(\mathbf{y})} = -2\omega^2 s_0(\mathbf{y}) G_0(\mathbf{y}, \mathbf{x}_r, \omega) G_0(\mathbf{x}, \mathbf{y}, \omega), \tag{12}$$

Then, we substitute equations (11) and (12) in the image derivative to get the result:

$$\begin{aligned}
&\frac{\partial I(\mathbf{x}, \mathbf{h})}{\partial s(\mathbf{y})}|_{s_0} = \\
&\sum_{\omega, \mathbf{x}_s, \mathbf{x}_r} \left\{-2\omega^2 s_0(\mathbf{y}) G_0^*(\mathbf{y}, \mathbf{x}_s, \omega) G_0^*(\mathbf{x} - \mathbf{h}, \mathbf{y}, \omega)\right\} G_0^*(\mathbf{x} + \mathbf{h}, \mathbf{x}_r, \omega) d(\mathbf{x}_r, \mathbf{x}_s, \omega) \\
+ &\sum_{\omega, \mathbf{x}_s, \mathbf{x}_r} \left\{-2\omega^2 s_0(\mathbf{y}) G_0^*(\mathbf{x} - \mathbf{h}, \mathbf{x}_s, \omega) G_0^*(\mathbf{x} + \mathbf{h}, \mathbf{y}, \omega)\right\} G_0^*(\mathbf{y}, \mathbf{x}_r, \omega) d(\mathbf{x}_r, \mathbf{x}_s, \omega).
\end{aligned} \tag{13}$$

Finally, we can express the image perturbation as the following:

$$\begin{aligned}
\Delta I(\mathbf{x}, \mathbf{h}) &= \sum_{\mathbf{y}} \frac{\partial I(\mathbf{x}, \mathbf{h})}{\partial s(\mathbf{y})} \Delta s(\mathbf{y}) \\
&= \sum_{\omega, \mathbf{x}_s, \mathbf{x}_r, \mathbf{y}} \left\{-2\omega^2 s_0(\mathbf{y}) G_0^*(\mathbf{y}, \mathbf{x}_s, \omega) G_0^*(\mathbf{x} - \mathbf{h}, \mathbf{y}, \omega)\right\} G_0^*(\mathbf{x} + \mathbf{h}, \mathbf{x}_r, \omega) d(\mathbf{x}_r, \mathbf{x}_s, \omega) \Delta s(\mathbf{y}) \\
&+ \sum_{\omega, \mathbf{x}_s, \mathbf{x}_r, \mathbf{y}} \left\{-2\omega^2 s_0(\mathbf{y}) G_0^*(\mathbf{x} - \mathbf{h}, \mathbf{x}_s, \omega) G_0^*(\mathbf{x} + \mathbf{h}, \mathbf{y}, \omega)\right\} G_0^*(\mathbf{y}, \mathbf{x}_r, \omega) d(\mathbf{x}_r, \mathbf{x}_s, \omega) \Delta s(\mathbf{y}),
\end{aligned} \tag{14}$$

Similarly, we can now compute the gradient, as given by:

$$\begin{aligned}
\Delta s(\mathbf{y}) &= \sum_{\mathbf{x},\mathbf{h}} \left(\frac{\partial I(\mathbf{x},\mathbf{h})}{\partial s(\mathbf{y})}|_{s_0} \right)^* \Delta I(\mathbf{x},\mathbf{h}) \\
&= \sum_{\omega,\mathbf{x}_s,\mathbf{x}_r,\mathbf{x},\mathbf{h}} \left\{ -2\omega^2 s_0(\mathbf{y}) G_0(\mathbf{y},\mathbf{x}_s,\omega) G_0(\mathbf{x}-\mathbf{h},\mathbf{y},\omega) \right\} G_0(\mathbf{x}+\mathbf{h},\mathbf{x}_r,\omega) d^*(\mathbf{x}_r,\mathbf{x}_s,\omega) \Delta I(\mathbf{x},\mathbf{h}) \\
&+ \sum_{\omega,\mathbf{x}_s,\mathbf{x}_r,\mathbf{x},\mathbf{h}} \left\{ -2\omega^2 s_0(\mathbf{y}) G_0(\mathbf{x}-\mathbf{h},\mathbf{x}_s,\omega) G_0(\mathbf{x}+\mathbf{h},\mathbf{y},\omega) \right\} G_0(\mathbf{y},\mathbf{x}_r,\omega) d^*(\mathbf{x}_r,\mathbf{x}_s,\omega) \Delta I(\mathbf{x},\mathbf{h}) \\
&= -2\omega^2 s_0(\mathbf{y}) \sum_{\omega,\mathbf{x}_s,\mathbf{x}_r} G_0(\mathbf{y},\mathbf{x}_s,\omega) d^*(\mathbf{x}_r,\mathbf{x}_s,\omega) \sum_{\mathbf{x},\mathbf{h}} G_0(\mathbf{x}-\mathbf{h},\mathbf{y},\omega) G_0(\mathbf{x}+\mathbf{h},\mathbf{x}_r,\omega) \Delta I(\mathbf{x},\mathbf{h}) \\
&- 2\omega^2 s_0(\mathbf{y}) \sum_{\omega,\mathbf{x}_s,\mathbf{x}_r} G_0(\mathbf{y},\mathbf{x}_r,\omega) d^*(\mathbf{x}_r,\mathbf{x}_s,\omega) \sum_{\mathbf{x},\mathbf{h}} G_0(\mathbf{x}+\mathbf{h},\mathbf{y},\omega) G_0(\mathbf{x}-\mathbf{h},\mathbf{x}_s,\omega) \Delta I(\mathbf{x},\mathbf{h}).
\end{aligned} \tag{15}$$

INTERPRETATION

There are several ways to interpret equations (14) and (15). For simplicity, let us first break each perturbation into two components, one from the source side and one from the receiver side. So, for equation (14), the first component will be as following:

$$\begin{aligned}
\Delta I_S(\mathbf{x},\mathbf{h}) = \sum_{\omega,\mathbf{x}_s} &\left\{ \sum_{\mathbf{y}} -2\omega^2 s_0(\mathbf{y}) G_0^*(\mathbf{y},\mathbf{x}_s,\omega) \Delta s(\mathbf{y}) G_0^*(\mathbf{x}-\mathbf{h},\mathbf{y},\omega) \right\} \\
&\left\{ \sum_{\mathbf{x}_r} G_0^*(\mathbf{x}+\mathbf{h},\mathbf{x}_r,\omega) d(\mathbf{x}_r,\mathbf{x}_s,\omega) \right\}.
\end{aligned} \tag{16}$$

Now, we can further break equation (16) into two components that we define as follows:

$$\Delta S(\mathbf{x}-\mathbf{h},\mathbf{x}_s,\omega) = -2\omega^2 \sum_{\mathbf{y}} s_0(\mathbf{y}) G_0(\mathbf{y},\mathbf{x}_s,\omega) \Delta s(\mathbf{y}) G_0(\mathbf{x}-\mathbf{h},\mathbf{y},\omega), \tag{17}$$

and

$$R_0(\mathbf{x}+\mathbf{h},\mathbf{x}_s,\omega) = \sum_{\mathbf{x}_r} G_0^*(\mathbf{x}+\mathbf{h},\mathbf{x}_r,\omega) d(\mathbf{x}_r,\mathbf{x}_s,\omega). \tag{18}$$

We can see that equation (17) represents the Born-modeled-wavefield due to the slowness perturbation and equation (18) represents the background receiver wavefield. So, we can now present the source side of the image perturbation as the following:

$$\Delta I_S(\mathbf{x},\mathbf{h}) = \sum_{\omega,\mathbf{x}_s} \Delta S_0^*(\mathbf{x}-\mathbf{h},\mathbf{x}_s,\omega) R_0(\mathbf{x}+\mathbf{h},\mathbf{x}_s,\omega). \tag{19}$$

Now, we can perform a similar analysis on the other component of equation (14), which is:

$$\Delta I_R(\mathbf{x},\mathbf{h}) = \sum_{\omega,\mathbf{x}_s} G_0^*(\mathbf{x}-\mathbf{h},\mathbf{x}_s,\omega)\{\sum_{\mathbf{y}} -2\omega^2 s_0(\mathbf{y}) G_0^*(\mathbf{x}+\mathbf{h},\mathbf{y},\omega)\Delta s(\mathbf{y})\} \{\sum_{\mathbf{x}_r} G_0^*(\mathbf{y},\mathbf{x}_r,\omega) d(\mathbf{x}_r,\mathbf{x}_s,\omega)\}. \tag{20}$$

Again, let us define a perturbed receiver wavefield and a background source wavefield as the following:

$$R_0(\mathbf{y},\mathbf{x}_s,\omega) = \sum_{\mathbf{x}_r} G_0^*(\mathbf{y},\mathbf{x}_r,\omega) d(\mathbf{x}_r,\mathbf{x}_s,\omega), \tag{21}$$

$$\Delta R(\mathbf{x}+\mathbf{h},\mathbf{x}_s,\omega) = -2\omega^2 \sum_{\mathbf{y}} s_0(\mathbf{y}) G_0^*(\mathbf{x}+\mathbf{h},\mathbf{y},\omega)\Delta s(\mathbf{y}) R_0(\mathbf{y},\mathbf{x}_s,\omega), \tag{22}$$

$$S_0(\mathbf{x}-\mathbf{h},\mathbf{x}_s,\omega) = G_0(\mathbf{x}-\mathbf{h},\mathbf{x}_s,\omega). \tag{23}$$

This enables us to represent the receiver side of the image perturbation as the following:

$$\Delta I_R(\mathbf{x},\mathbf{h}) = \sum_{\omega,\mathbf{x}_s} S_0^*(\mathbf{x}-\mathbf{h},\mathbf{x}_s,\omega)\Delta R(\mathbf{x}+\mathbf{h},\mathbf{x}_s,\omega). \tag{24}$$

As for equation (15), we do the same analysis to arrive at the following gradient formulae:

$$\Delta s_R(\mathbf{y}) = \sum_{\omega,\mathbf{x}_s} S_0(\mathbf{y},\mathbf{x}_s,\omega)\Delta R^*(\mathbf{y},\mathbf{x}_s,\omega), \tag{25}$$

$$\Delta s_S(\mathbf{y}) = \sum_{\omega,\mathbf{x}_s} \Delta S(\mathbf{y},\mathbf{x}_s,\omega) R_0^*(\mathbf{y},\mathbf{x}_s,\omega), \tag{26}$$

where the residual wavefields are defined as the following:

$$\Delta R(\mathbf{y},\mathbf{x}_s,\omega) = -2\omega^2 \sum_{\mathbf{x},\mathbf{h}} s_0(\mathbf{y}) G_0^*(\mathbf{x}-\mathbf{h},\mathbf{y},\omega)\Delta I(\mathbf{x},\mathbf{h}) R_0(\mathbf{x}+\mathbf{h},\mathbf{x}_s,\omega), \tag{27}$$

$$\Delta S(\mathbf{y},\mathbf{x}_s,\omega) = -2\omega^2 \sum_{\mathbf{x},\mathbf{h}} s_0(\mathbf{y}) G_0(\mathbf{x}+\mathbf{h},\mathbf{y},\omega) G_0(\mathbf{x}-\mathbf{h},\mathbf{x}_s,\omega)\Delta I(\mathbf{x},\mathbf{h}). \tag{28}$$

In summary, the tomographic operator computes the image perturbation or slowness perturbation by correlating background and residual wavefields of both source and receiver sides.

SYNTHETIC EXAMPLES

Although the derivation was performed in the frequency-domain, we will apply the tomographic operator in the time-domain. First, we will start with a simple example with a constant background velocity of 2500 m/s. The spatial sampling is 10 m and the temporal sampling is 2 ms. A Ricker wavelet with a fundamental frequency of

20 Hz is used to model the data. There is one reflector at the bottom of the model at a depth of 900 m. Now, we will input a slowness perturbation to the forward operator to generate a corresponding image perturbation. Three slowness perturbations are supplied. First, a spike located at a depth of 400 m. Second, a vertical line extending from a depth of 300 m to 500 m. Third, a horizonal line at a depth of 400 m. The three slowness perturbations are shown in Figure 1. We apply the forward tomographic operator on these slowness perturbations to get the corresponding image perturbations. Figure 2 shows the image perturbation (at zero subsurface offset only). Then, we apply the adjoint tomographic operator to these image perturbations to recreate the slowness perturbations. The results of applying the adjoint scattering operator are shown in Figure 3. As expected, the reconstructed slowness perturbations have higher horizontal resolution than vertical resolution. Figure 4 shows the amplitude spectrum of the recreated slowness perturbation in Figure 3(a).

For a second test, we will repeat a similar experiment but with a different background velocity model. As shown in Figure 5, the velocity model includes areas of low velocity to the top, and areas of high velocity in the middle, representing a salt body. There is one reflector at the bottom of the model at a depth of 3500 m. The spatial sampling is 25 m and the temporal sampling is 4 ms. A Ricker wavelet with a fundamental frequency of 10 Hz is used to model the data. The slowness perturbation is a spike located at a depth of 2600 m, which is located in between the reflector and the salt body. The corresponding image perturbation resulted from applying the forward tomographic operator is shown in Figure 6(a) and the reconstructed slowness perturbation is shown in Figure 6(b). Figure 6(c) shows the amplitude spectrum of the reconstructed slowness perturbation. The change in the background velocity affected the reconstructed slowness perturbation, both in physical space and in Fourier space.

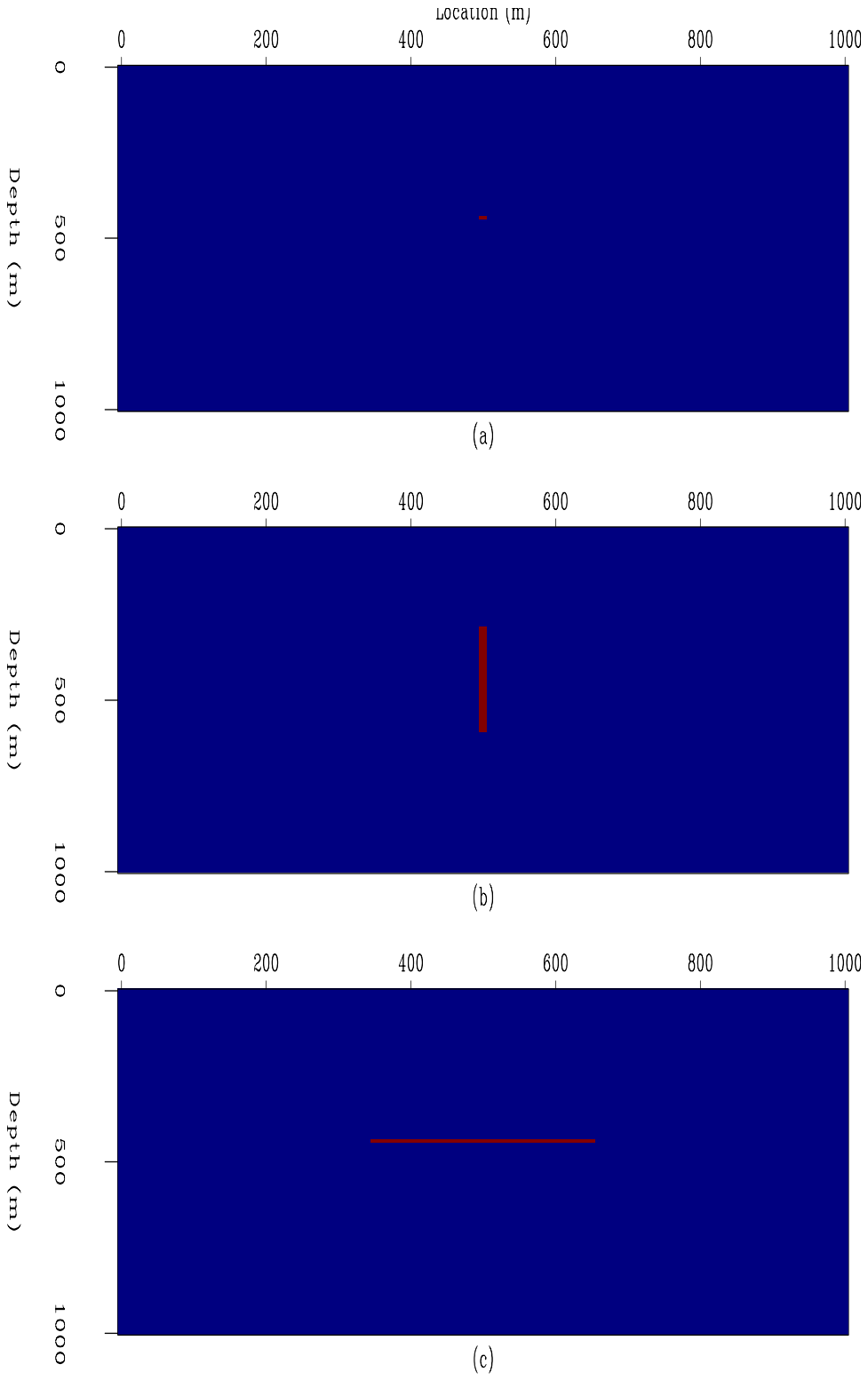

Figure 1: Three slowness perturbations that will be used in the forward operator. [**ER**]

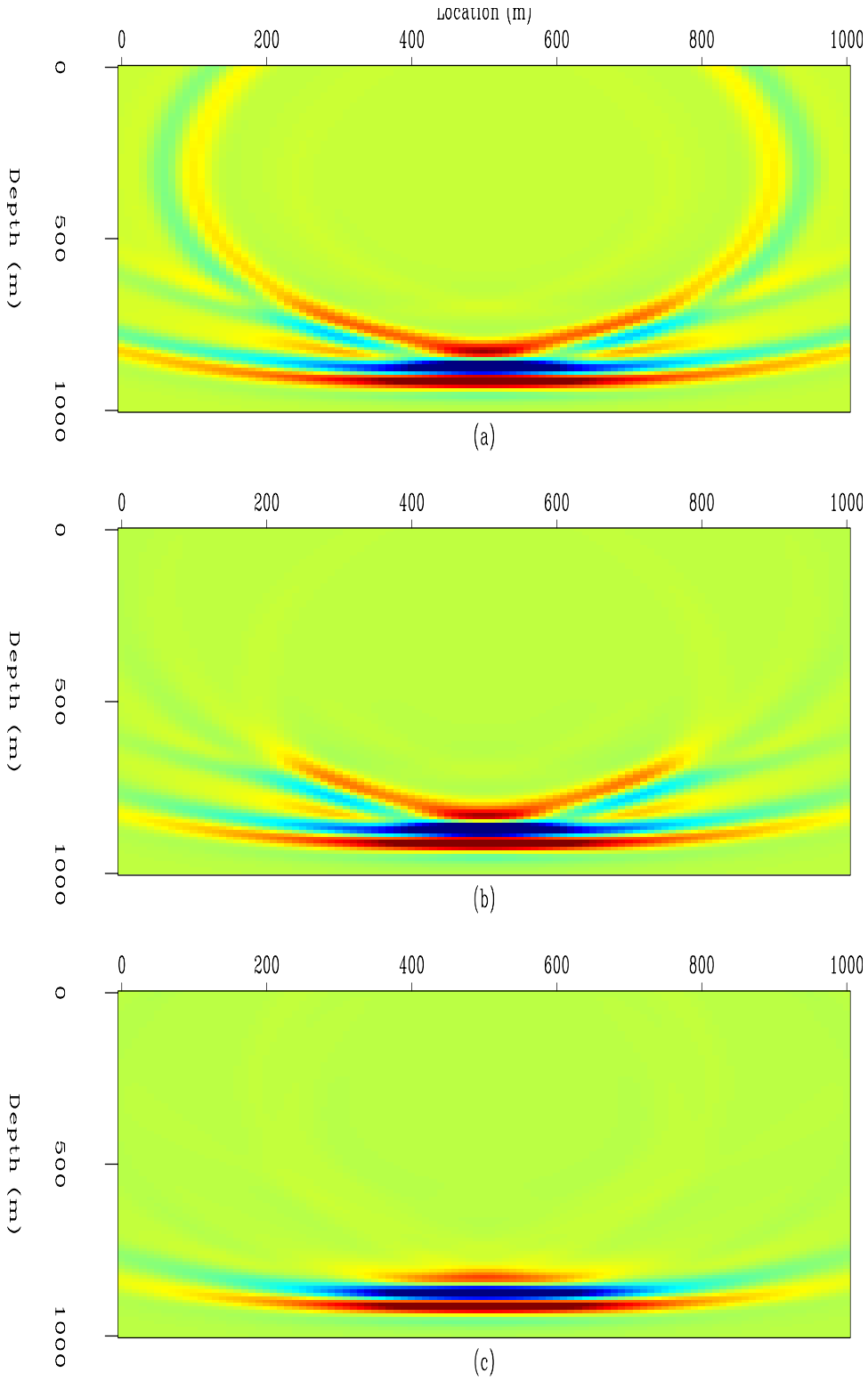

Figure 2: The three image perturbations corresponding to slowness perturbations in Figure 1, produced by the forward scattering operator. [**ER**]

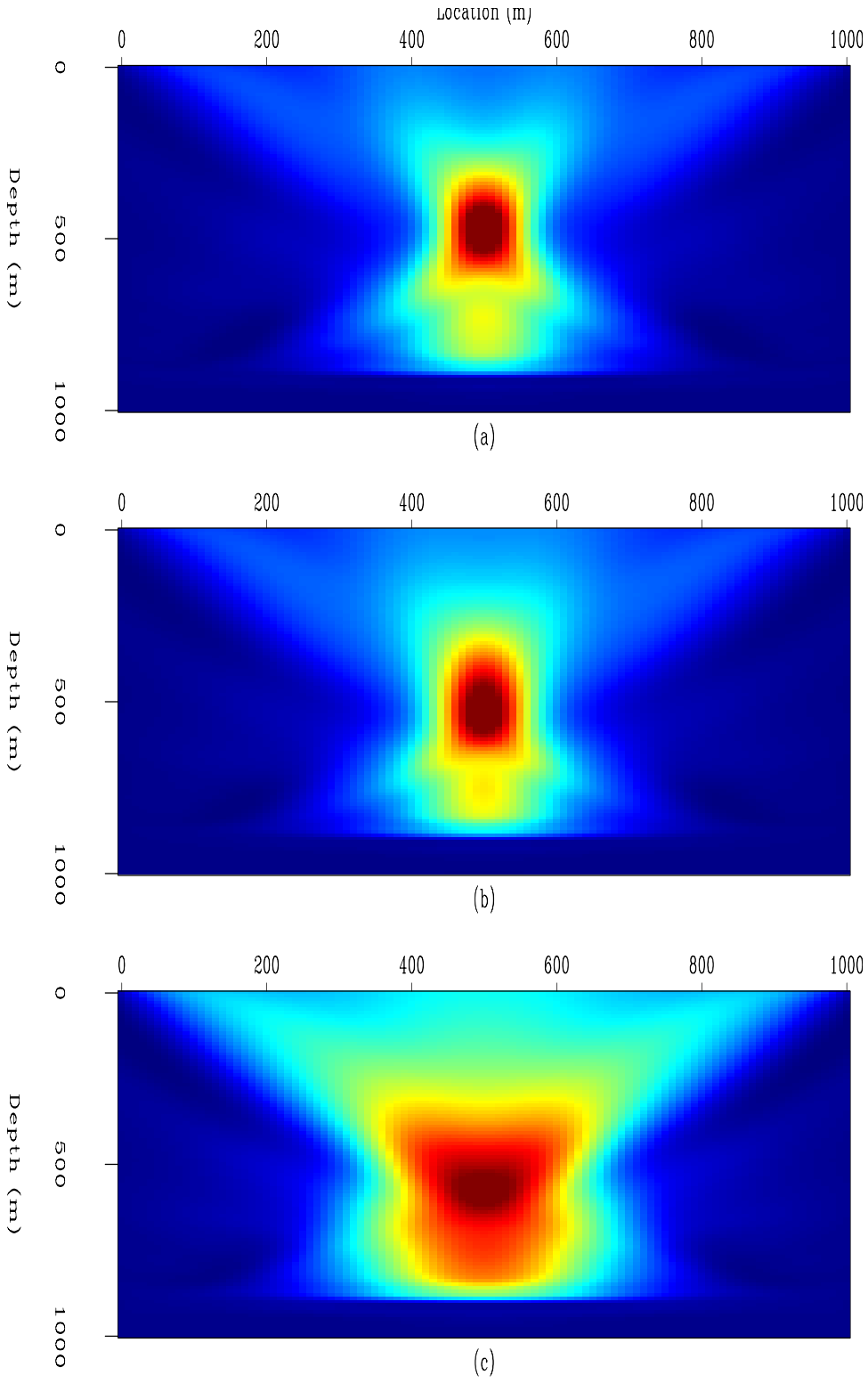

Figure 3: The reconstructed slowness perturbations by the adjoint scattering operator. [**ER**]

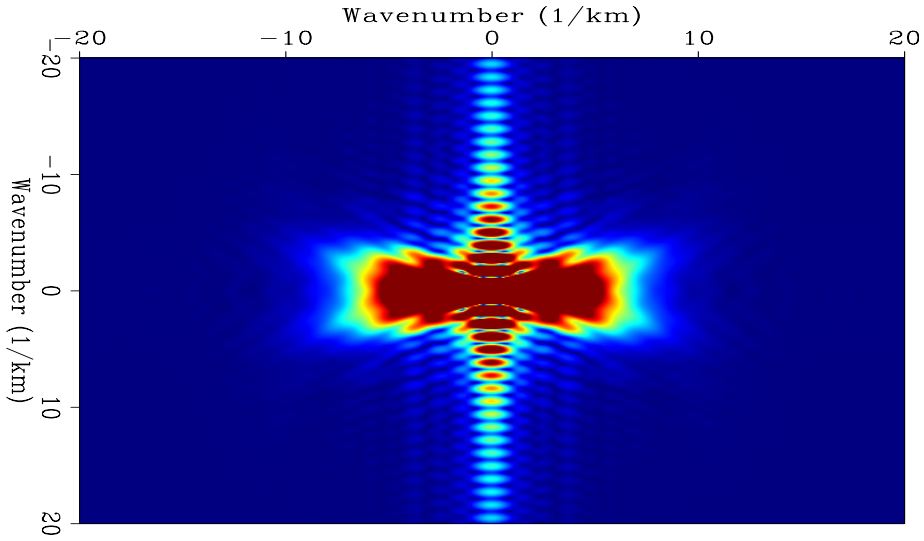

Figure 4: The Fourier transform of spike response in Figure 3(a). [**ER**]

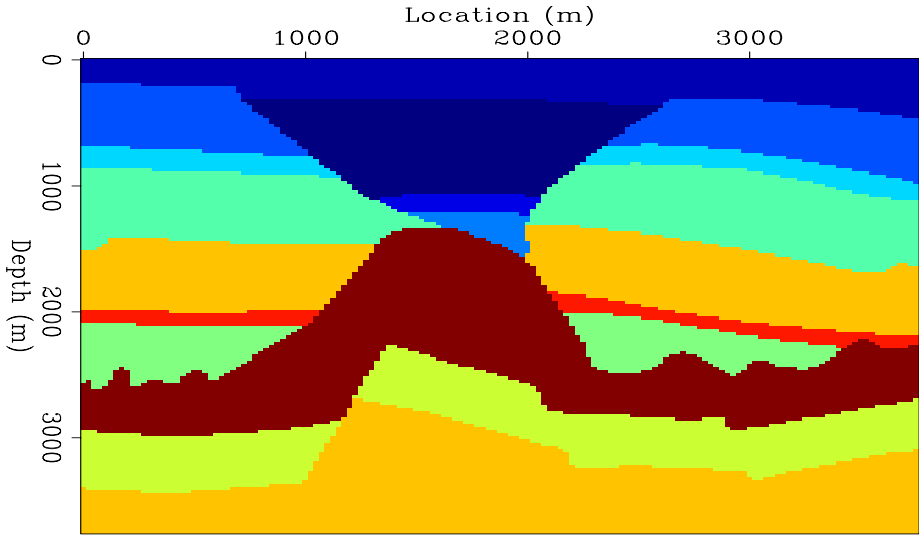

Figure 5: The background velocity model for the second test. [**ER**]

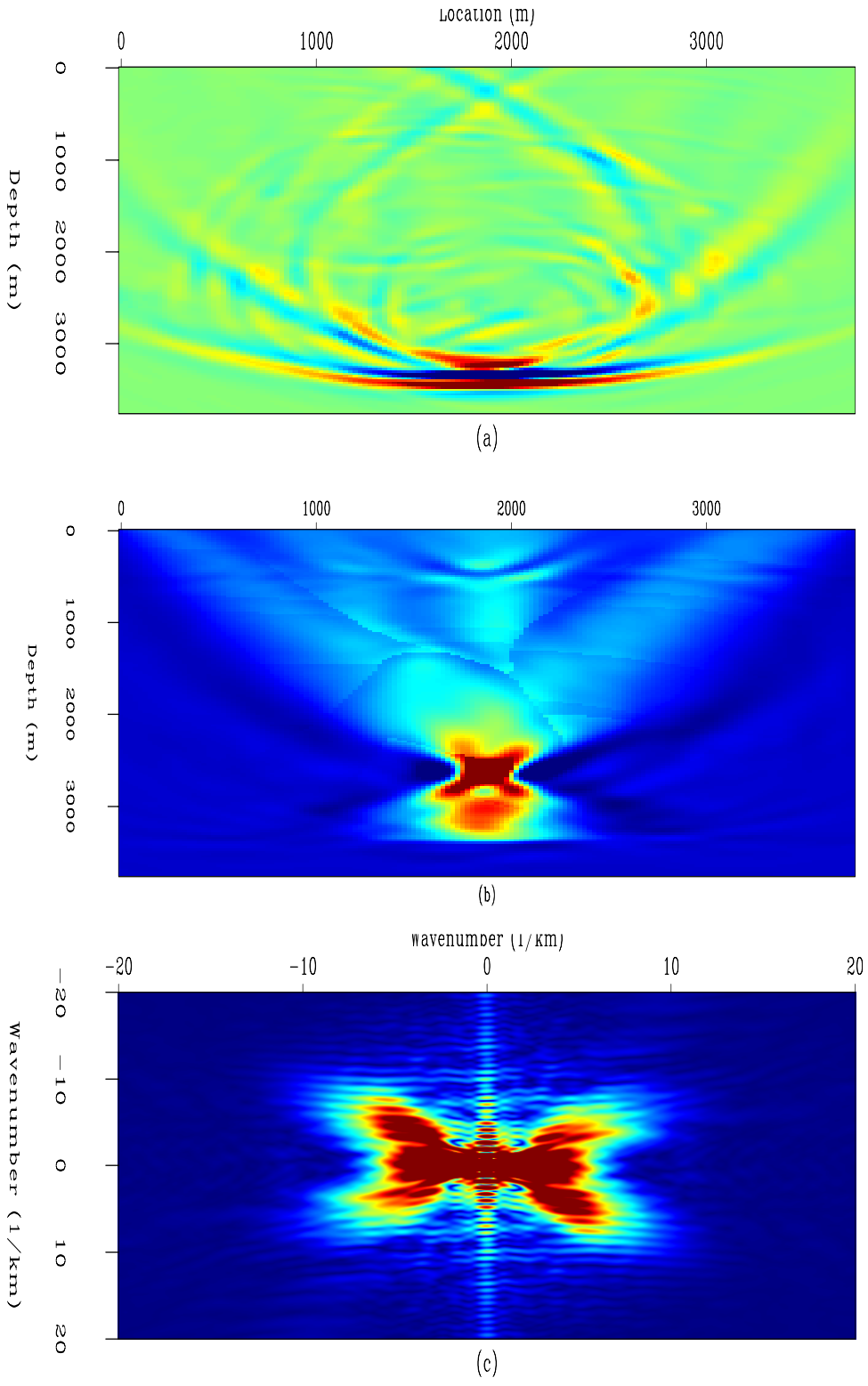

Figure 6: Using the background velocity in Figure 5, (a) the image perturbation, (b) reconstructed slowness perturbation, and (c) the Fourier transform for the reconstructed slowness perturbation. [**ER**]

CONCLUSIONS

In this paper, we derived the tomographic operator for wave equation migration velocity analysis tools based on the two-way wave equation. Only two approximations were used to derive the tomographic operator. Then, we tested the operator using two synthetic velocity models: first with constant velocity, and second with a more complex model that includes a high velocity salt body. The operator seems to give satisfactory results in both physical and Fourier spaces.

FUTURE WORK

The tomographic operator we derive can potentially produce superior results to the operators based on one-way wave equation since it can capture wave paths with more accuracy. So, the next step is to test the migration velocity estimation results on a complex synthetic model, where one-way propagation operators fail and measure the amount of improvement. Then, the velocity estimation process should be tested on a real dataset.

Finally, since this method is very computationally intensive, it is crucial to adapt it on accelerated and parallel processing units such as GPUs. This is especially attractive since GPUs are particularly efficient for finite-difference-based convolution algorithms such as propagation in time domain.

REFERENCES

Biondi, B., 2009, Measuring image focusing for velocity analysis: SEP-Report, **138**, 59–80.

———, 2010, Wave-equation migration velocity analysis by residual moveout fitting: SEP-Report, **142**, X–Y.

Biondi, B. and P. Sava, 1999, Wave-equation migration velocity analysis: SEG Technical Program Expanded Abstracts, **18**, 1723–1726.

Luo, Y. and G. T. Schuster, 1990, Wave-equation traveltime inversion: SEG Expanded Abstracts.

Shen, P., 2004, Wave equation migration velocity analysis by differential semblance optimization: PhD thesis, Rice University.

Symes, W. W. and J. J. Carazzone, 1991, Velocity inversion by differential semblance optimization: Geophysics, **56**, 654–663.

Tang, Y., C. Guerra, and B. Biondi, 2008, Image-space wave-equation tomography in the generalized source domain: SEP-Report, **136**, 1–22.

Tarantola, A., 1984, Inversion of seismic reflection data in the acoustic approximation: Geophysics, **49**, 1259–1266.